THE ASTROPHYSICAL JOURNAL, 342:769–784, 1989 July 15

RADIO STUDIES OF THE GALACTIC CENTER. I. THE SAGITTARIUS A COMPLEX

A. PEDLAR
Nuffield Radio Astronomy Laboratories, Jodrell Bank
K. R. ANANTHARAMAIAH,[1] R. D. EKERS, W. M. GOSS, AND J. H. VAN GORKOM[2]
National Radio Astronomy Observatory, Socorro
U. J. SCHWARZ
Kapteyn Astronomical Institute, Groningen
AND
JUN-HUI ZHAO
Department of Physics and Astronomy, University of New Mexico
Received 1988 October 24; accepted 1988 December 28

ABSTRACT

We present 90 cm, 20 cm, and 6 cm VLA observations of the Sgr A complex. The 90 cm measurements have a resolution of 12″ and the two shorter wavelength observations have a resolution of 2.″5 × 1.″3. These data have been combined, to obtain spectral index and optical depth distributions across the source. We have used the observations to constrain the three-dimensional structure at the Galactic center. At 90 cm the "spiral" structure of the thermal source Sgr A West is clearly seen in absorption ($\tau > 4$) against the nonthermal emission of Sgr A East, showing conclusively that Sgr A West is in front of Sgr A East. In addition the entire shell of Sgr A East shows a low-frequency turnover corresponding to an optical depth of $\sim$1–2. This turnover corresponds to free-free absorption with an emission measure of $\sim 10^5$ pc cm^{-6} if the electron temperature is $\sim$5000 K. The $\sim$7′ halo surrounding Sgr A East and West also shows a low-frequency turnover. We suggest that the halo contains a mixture of thermal and nonthermal gas and that the thermal component is responsible for the absorption extending across Sgr A East. The compact source at the Galactic center is not detected at 90 cm, suggesting that it is either behind or embedded in the ionized gas associated with Sgr A West. Two scenarios are considered to explain the properties of Sgr A: (1) ongoing star formation in which the radio emission is a direct consequence of supernovae, and (2) activity caused by a central engine (Sgr A*?) which shows similarities to the structures seen in more active spiral nuclei.

Subject headings: galaxies: nuclei — galaxies: The Galaxy — interferometry

I. INTRODUCTION

The central region of our Galaxy exhibits the qualitative properties of a mildly active galactic nucleus (AGN), even though the energies are several orders of magnitude less than conventional members of this class. However, the complex at the center of our Galaxy can be studied on linear scales hundreds of times smaller than the nearest extragalactic AGN. Because of this difference in linear resolution, most nearby AGN in spiral galaxies appear to have a deceptively simple radio structure consisting of a few discrete components (Ulvestad and Wilson 1984; Unger *et al.* 1986), whereas the radio structure of the center of our Galaxy shows a variety of phenomena ranging from the "arc" feature, which consists of linear, parallel filaments (Yusef-Zadeh, Morris and Chance 1984), and extensive "threads" of radio emission (Morris and Yusef-Zadeh 1985) to the extremely compact ($\sim$20 AU) source (Balick and Brown 1974; Lo and Claussen 1984) designated SgrA*.

The most intriguing structure, however, is Sagittarius A (Sgr A) itself, which Ekers *et al.* (1983) showed to consist of a thermal "spiral" (Sgr A West), apparently centered on Sgr A*, and a nonthermal shell (Sgr A East). Both components are surrounded by an extensive "halo" with an angular size of $\sim$7′. This region, "the Sgr A complex," contains a number of additional structures which are described in a recent extensive study at 20 cm by Yusef-Zadeh and Morris (1987). It seems clear that Sgr A West is physically associated with the actual nucleus of our Galaxy (e.g., Oort 1985). However, it is not clear whether Sgr A East originates from activity at the Galactic center, or is just a chance superposition of a supernova remnant along the line of sight. The three-dimensional structure in this region of the Galaxy is particularly difficult to determine, as Galactic rotation cannot be used to estimate distances. Molecular and atomic line absorption studies have been used as a diagnostic of the geometry of the region and Güsten and Downes (1980) suggested that both Sgr A East and West were interior to the molecular ring (i.e., within a few hundred pc of the center), but separated by at least 100 pc with the +40 km s^{-1} molecular cloud situated between them. However, high-resolution H_2CO absorption measurements by Whiteoak, Gardner, and Pankonin (1983) showed the +40 km s^{-1} cloud to be in absorption against Sgr A West which is inconsistent with the above model. Liszt *et al.* (1983) detected neutral hydrogen absorption at +40–60 km s^{-1} against the compact source but not against Sgr A West, but they interpreted this as evidence for the patchiness of the hydrogen rather than evidence that the components were spatially separate.

The radio continuum emission of Sgr A consists of a mixture of thermal free-free and nonthermal, presumably synchrotron, emission. At centimeter wavelengths both components are

[1] On leave from the Raman Research Institute, Bangalore, India.
[2] Also at Columbia University.

optically thin, and it is not possible to use such measurements to determine the relative positions of individual components along the line of sight. Previous low-frequency radio studies (e.g., Little 1974; Dulk and Slee 1974; Mills and Drinkwater 1984; Yusef-Zadeh *et al.* 1986) have shown that the thermal component in Sgr A becomes increasingly opaque at long wavelengths, and at 375 cm the source has disappeared completely (LaRosa and Kassim 1985). Hence the increase in optical depth of the thermal component at low frequencies can be used to constrain the three-dimensional structure of the Galactic center. In addition the high brightness temperature of the nonthermal background at low frequencies enables us to detect ionized gas with lower emission measures than can be detected at higher frequencies. For example, in a 12″ beam if the brightness temperature of the background at 90 cm is 10^5 K, then thermal gas, at a temperature of 5000 K having an optical depth of 0.1, corresponding to an emission measure of $\sim 10^4$ pc cm^{-6}, will show absorption of ~ 120 mJy per beam, whereas at 2 cm the same gas will show emission of only ~ 5 mJy per beam.

In this paper we present observations of the Sgr A complex made using the VLA (Thompson *et al.* 1980) at 90 cm with an angular resolution of 12″. In addition we present 6 and 20 cm VLA observations with an angular resolution of 1.″3 × 2.″5. The 6 and 20 cm images are formed by combining data from B, C, and D and A, B, C, and D arrays, respectively, and hence are well suited to the study of extended structure in the Sgr A complex. Intermediate resolution 2 cm observations have been used to constrain the properties of the thermal free-free emission. We combine all observations to obtain the $\lambda 90/20$ spectral index α ($S_\nu = S_0 \nu^\alpha$) and 90 cm optical depth distributions with a resolution of 12″. Assuming the Galactic center to be at 10 kpc, this gives a linear resolution of 0.6 pc enabling the details of the major components of the Sgr A region to be separated.

In § II, we present the observing procedures and data reduction techniques. The results of the observations are presented in § III. In § IV, we present the interpretation of the results and discuss some implications. Our results and conclusions are summarized in § V.

II. THE OBSERVATIONS AND REDUCTION

a) The 90 Centimeter Data

The observations presented in this paper were obtained during a study of low-frequency (H270α) recombination lines toward the Galactic center using the VLA. Although at the start of the project only 10 antennas had been equipped with 90 cm receivers, this number increased to 15 for the later observations. Four separate observing runs, nominally in the A, B, C, and D configurations, respectively, were carried out between 1986 March and 1987 May (see Table 1). All the observations were made in spectral line mode which allows the option of removing channels, affected by narrow-band interference, before forming the continuum data bases. A central frequency of 332.380 MHz was selected to include the H270α line. The FWHM of the primary beam at 332 MHz is 2.°6. In order to map sources near the edge of the beam without significant bandwidth smearing effects (Cotton 1985), narrow-band continuum databases were made by combining interference-free channels (see Table 1). Short (10 s) integration times were used in the A and B array observations to reduce time-smearing effects. Longer integration times and wider bandwidths were employed for the more compact C and D array observations where time-smearing and bandwidth-smearing effects are less important. Typically, Sgr A was tracked for 8 hr per array, and the combination of all four arrays gave reasonable coverage of the Fourier (UV) plane up to spacings of 20,000 wavelengths (20 kλ), corresponding to an angular resolution of 12″. Between 20 and 35 kλ the Fourier plane is only sparsely sampled. The observations were amplitude-calibrated using 3C 286 which was assumed to have a flux density of 26.8 Jy at 332 MHz. The instrumental and ionospheric phase was calibrated using the compact source 1938−155. Data from the A and B array observations were edited and combined, and self-calibration techniques (Cornwell 1985) were used to correct the phases further. However, the lack of significant unresolved flux density on the longer baselines resulted in uncertain phase solutions beyond spacings of 20 kλ. Hence, although the longest spacings observed corresponded to a nominal resolution of 5″, the resulting images at this resolution were felt to be unreliable and a restoring beam of 12″ was used. Data from the C and D arrays were combined and the phase errors corrected by self-calibration. The resultant image of the combined C and D array data, with a resolution of 97″ × 54″, is shown in Figure 1. Finally the self-calibrated data from the compact (C and D) and extended (A and B) arrays were combined and Fourier transformed. The resulting image was deconvolved using the Steer-Dewdney-Ito (1984) clean algorithm.

The final image, which has been restored with a 12″ circular Gaussian beam, is shown in Figure 2 (Plate 13). In order to

TABLE 1

OBSERVING LOG

Wavelength (cm)	Bandwidth (MHz)	Mean Frequency (MHz)	Array (Number of Antennas)	Date
90	0.7	332	A (11)	1986 Mar
	1.17	332	B (7)	1986 Aug
	1.17	332	C (15)	1986 Dec
	1.17	332	D (15)	1987 May
20	2 × 25	1452 and 1502	A (27)	1983 Oct
	25	1452	B (27)	1981 Jun
	2 × 25	1452 and 1502	C (27)	1984 May
	25	1452 and 1502	D (27)	1984 Aug
6	50	4865	B (27)	1982 Oct
	50	4865	C (27)	1981 Dec
	2 × 25	4623 and 4873	D (27)	1984 Aug
2	2 × 50	14915 and 14965	D (27)	1983 Jul

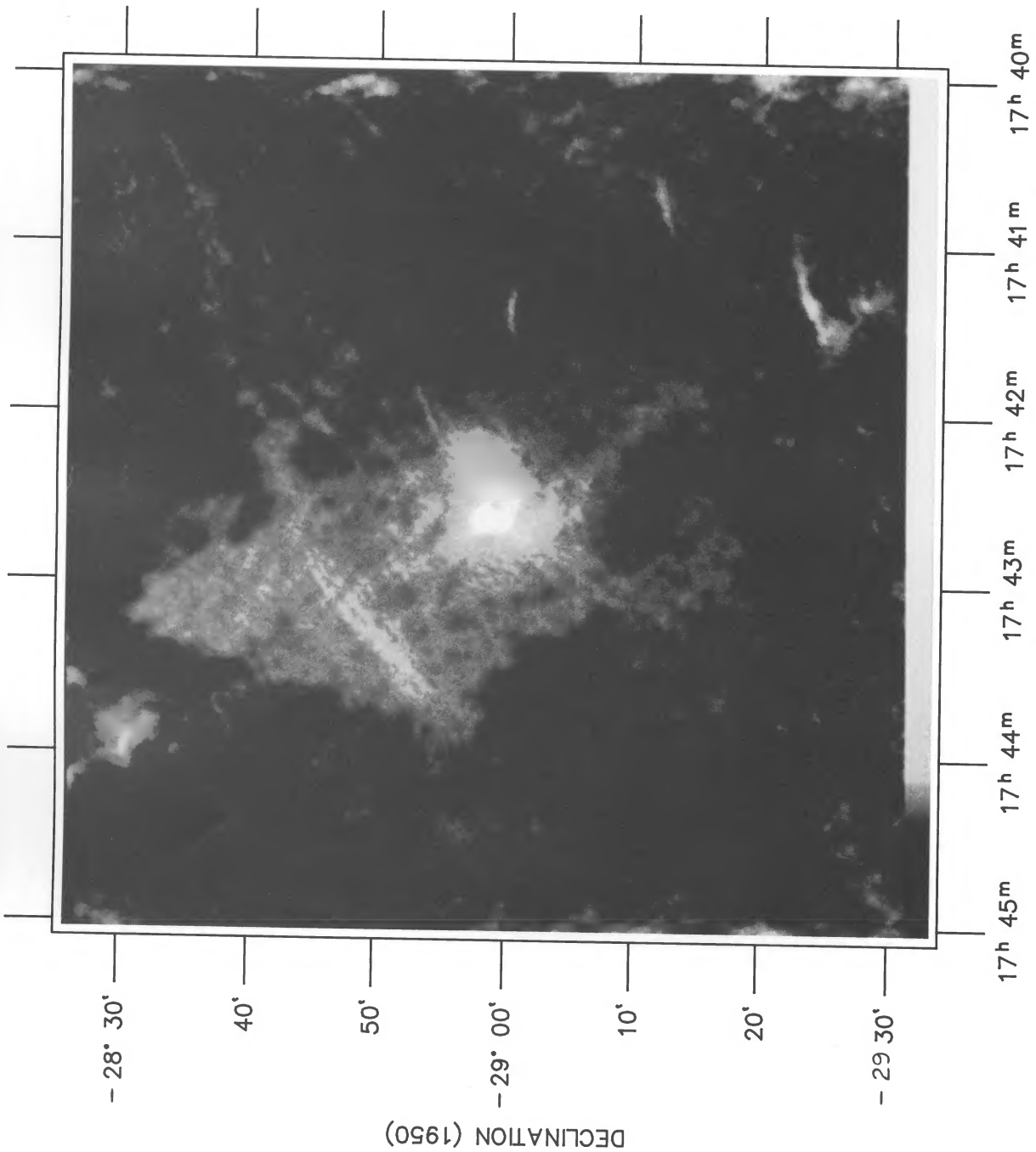

FIG. 2.—A gray scale representation of the 90 cm image obtained using data combined from A, B, C, and D array observations. The restoring beam is a circular Gaussian with a HPBW of 12″. A histogram-equalizing transfer function has been used to display this image (Rots 1985). The markings on the gray scale code at the bottom left corner are 0.0, 0.5, and 1.0 Jy per beam.

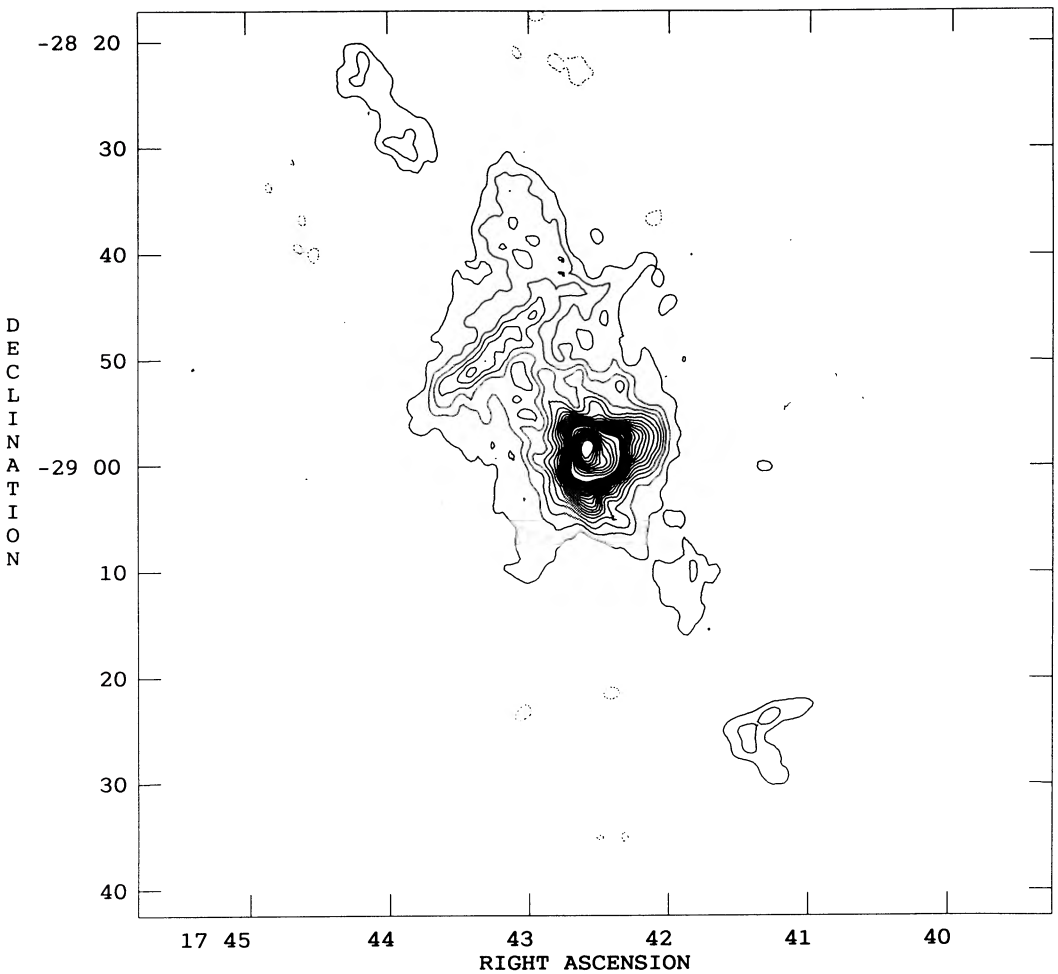

FIG. 1.—The 90 cm image produced using the more compact (C and D) arrays only. The restoring beam is a Gaussian with HPBW 97″ × 54″ in PA 11°.6. Contour levels are separated by 0.4 Jy per beam up to 8 Jy, and then 2.5 Jy per beam up to the maximum brightness of 36.6 Jy per beam.

bring out all the features, we have used a histogram-equalized transfer function (Rots 1985) to display the image. Figure 2 shows most of the features of the Galactic center region seen at higher frequencies. In addition to Sgr A and the Arc, both Sgr B2, Sgr B1, and Sgr C are evident in the image. A number of weak features such as the "threads" (Morris and Yusef-Zadeh 1985) can also be identified by comparison with higher frequency images, although the "arched filaments" are barely detectable. An interesting new feature is a loop like structure to the south of the Sgr A complex. The image is limited to a dynamic range of 100:1, largely due to insufficient UV coverage, phase errors, and the difficulties caused by noncoplanar baselines (Perley 1988). Hence some of the fine structure seen in Figure 2 should be treated with caution. Spacings shorter than $\sim 100\lambda$ are missing, and only ~900 Jy is detected from the central 50′ in Figure 1, whereas single-dish measurements (Pedlar *et al.* 1978) indicate ~2000 Jy from this region. However, as this paper is only concerned with the central 10′, the lack of information on extended structure greater than ~30′ will not seriously affect our conclusions. The missing flux density only corresponds to an average offset of ~20 mJy per beam. The rms noise achieved in the combined image was 16 mJy per beam, which at 90 cm corresponds to a brightness temperature of ~1300 K.

b) The 20 Centimeter and 6 Centimeter Data

These data were obtained in a number of observing sessions in 1981–1984, details of which are summarized in Table 1. The 20 cm B array and 6 cm C array data are those discussed by Ekers *et al.* (1983). The calibration was carried out using the method described by Ekers *et al.*, the flux density being set with respect to 3C 286. The data were initially calibrated using 1748−253, and the self-calibration procedure (Cornwell 1985) was used to further correct each data set. The primary beams were 30′ at 20 cm and 10′ at 6 cm.

The final images at 6 cm (B, C, and D arrays combined) and 20 cm (A, B, C, and D arrays combined) have been restored with a 1″.3 × 2″.5 ($\alpha \times \delta$) beam. The deconvolution algorithms used were the Steer-Dewdney-Ito (1984) CLEAN procedure for the 6 cm image and the multiresolution CLEAN procedure (Wakker and Schwarz 1988) using two smoothing steps, for the 20 cm image. The total flux density of the Sgr A complex at 20 cm is 487 ± 30 Jy, where the error represents the difficulty in separating the halo from the background emission. This value is substantially larger than that presented by Ekers *et al.* and represents contributions from the larger scale structure measured by the more compact arrays. When convolved down to a resolution of 10″ the image agrees well with the 20 cm image

shown in Figure 4 of Yusef-Zadeh and Morris (1987), and the peak intensities agree within 7%. These images are still limited by lack of spacings less than 40 m, and hence extended structure larger than 18′ at 20 cm, and 5′ at 6 cm, will be missed.

The full-resolution 6 cm and 20 cm images are shown in Figures 3 and 4. The rms noise in the 6 cm image is 0.4 mJy per beam and 1.3 mJy per beam in the 20 cm image. These images contain no polarization information since some of the observations were taken in spectral line mode. The 3 σ limits for the fractional polarization are $<2.3\%$ at 6 cm and $<1\%$ at 20 cm for C and B array observations, respectively.

c) *The 2 Centimeter Data*

These data, which will be used in the present paper mainly to estimate the thermal contribution, was obtained in 1983 in an attempt to measure polarization from the shell of Sgr A East. A 7 hr observation using the VLA D configuration was used, and the field center was $\alpha = 17^h42^m33^s.0$, $\delta = -29°59'00''$. The data were self-calibrated and the rms noise is 1.6 mJy in stokes parameter I and 0.24 mJy in Q, where the restoring beam is $3''.2 \times 6''.5$ ($\alpha \times \delta$).

After correcting for primary beam (3′.5 FWHM) attenuation, we measure the flux density of Sgr A West to be 17 ± 2 Jy and Sgr A East to be 11 ± 4 Jy, although as missing zero order spacings results in lack of sensitivity to extended structure on scales greater than 2′, these values should be considered as lower limits, particularly for Sgr A East. The polarization of Sgr A East at 2 cm was found to be less than 6%.

III. THE RESULTS

a) *The 90 Centimeter Image*

In this paper, we shall discuss only the central region which includes Sgr A East and West superposed on a $\sim 7'$ halo. This central part of the 90 cm image, together with the 20 cm image convolved to the same resolution, is shown in Figure 5. The properties of the extended field at 90 cm will be discussed in a later paper. The brightest component in the 90 cm image is the

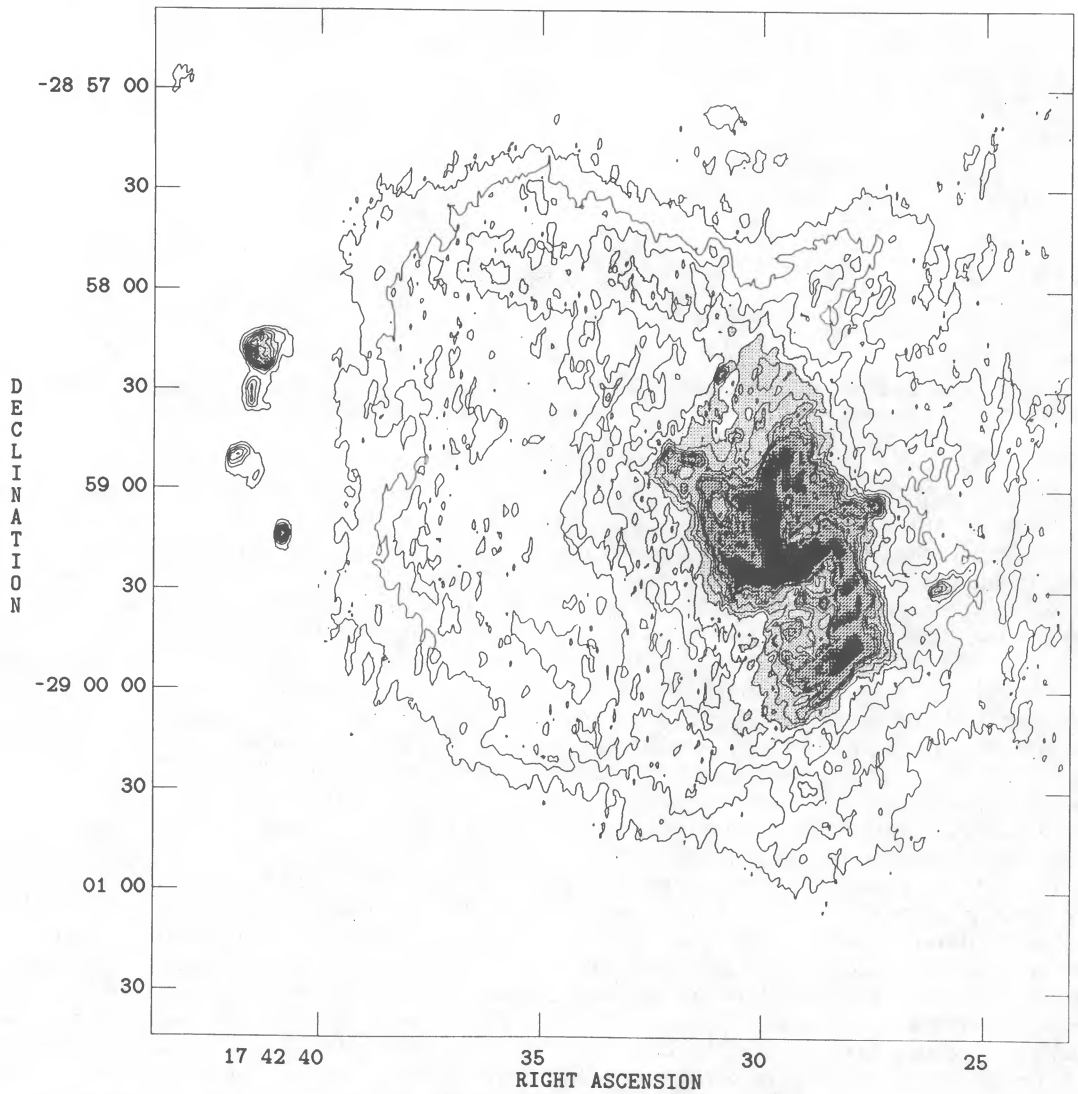

FIG. 3.—A contour plot of the central part of the 6 cm image. The restoring beam used was $1''.3 \times 2''.5$ ($\alpha \times \delta$), and the contour intervals are 3 mJy per beam up to 30 mJy per beam, 10 mJy per beam between 30 and 100 mJy per beam, and 20 mJy per beam thereafter. The peak flux density is 672 mJy per beam.

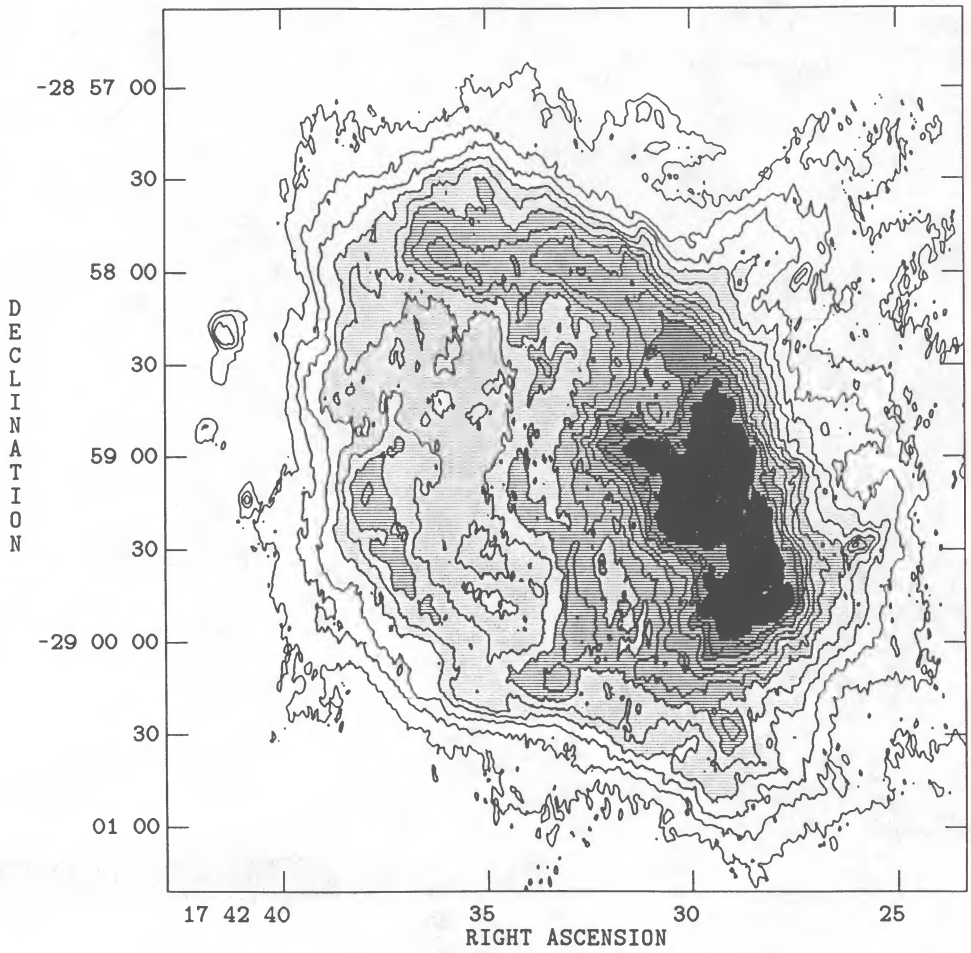

FIG. 4.—A contour plot of the central part of the 20 cm image. The restoring beam was 1.″3 × 2.″5 ($\alpha \times \delta$), and the contour intervals are at 5 mJy per beam up to 120 mJy per beam, and thereafter at 20 mJy per beam. The peak flux density is 467 mJy per beam.

2.′1 × 3.′3 shell (PA ~ 40°) identified with Sgr A East. This feature is situated on a roughly triangular-shaped halo with an extent of ~7′. The most striking feature, however, is the deep depression in the brightness on the western side of the shell, which is consistent with free-free absorption of Sgr A East by thermal gas associated with Sgr A West. This depression is particularly clearly seen by comparing Figure 5*a* with the same resolution 20 cm image in Figure 5*b*. The structure of the outer parts of the thermal spiral is evident in the absorption feature (Fig. 6), although that of the central parts have been hidden by extended absorption. As well as the Sgr A West absorption, the shell of Sgr A East encloses a weak linear emission feature, elongated approximately north-south, which is close to the eastern boundary of the absorption feature associated with Sgr A West (see Fig. 5*a*). The position of this feature is $\alpha \sim 17^h42^m34^s$, $\delta \sim -28°59'$. This feature is also seen in the 6 cm and 20 cm images (see § III*b*). The eastern edge of the shell is remarkably straight, which may be a consequence of its interaction with the +50 km s^{-1} molecular cloud (M−0.02−0.07) as suggested by Goss *et al.* (1985), Ho *et al.* (1985), and Mezger *et al.* (1988).

The ~7′ extended region (Sgr A halo) includes a ~1′ feature at $\alpha = 17^h42^m40^s$, $\delta = -29°01'$, together with a pronounced depression at the position of the eastern cluster of H II regions. It also encloses the "northwest streamers" identified at 20 cm by Yusef-Zadeh and Morris (1987), a system of filaments which extend ~3′ to the northwest of Sgr A*. At 90 cm these "streamers" appear to be an integral part of the general halo emission.

Parts, or all, of the Sgr A halo are often included in low-resolution flux density measurements of Sgr A. Even with the present high-resolution observations, it is difficult to separate this emission accurately from the general background. By inspection of crosscuts (e.g., Fig. 7), we deduce a background level between 50 and 100 mJy per beam at 90 cm, and, after removing this, measure a total flux density (Sgr A + halo) at 90 cm of 370 ± 50 Jy within the 10′ × 10′ field shown in Figure 5.

In view of the diffuse nature of Sgr A and its halo, caution must be exercised when comparing flux density measurements made by different instruments. Occultation measurements with an effective resolution of about 1′ (Gopal-Krishna, Sarma, and Joshi 1972), indicate a 92 cm flux density for this region of 165 ± 30 Jy and the 56″ resolution 92 cm Culgoora image (Yusef-Zadeh *et al.* 1986) gives a flux density of 200 Jy. However, it is clear from the present measurements that both these estimates do not include all the halo emission. The derived flux density depends critically on the assumed background level, and values agreeing with the above estimates can be obtained from our data by choosing different base levels. We shall discuss this problem further in § IV*a*.

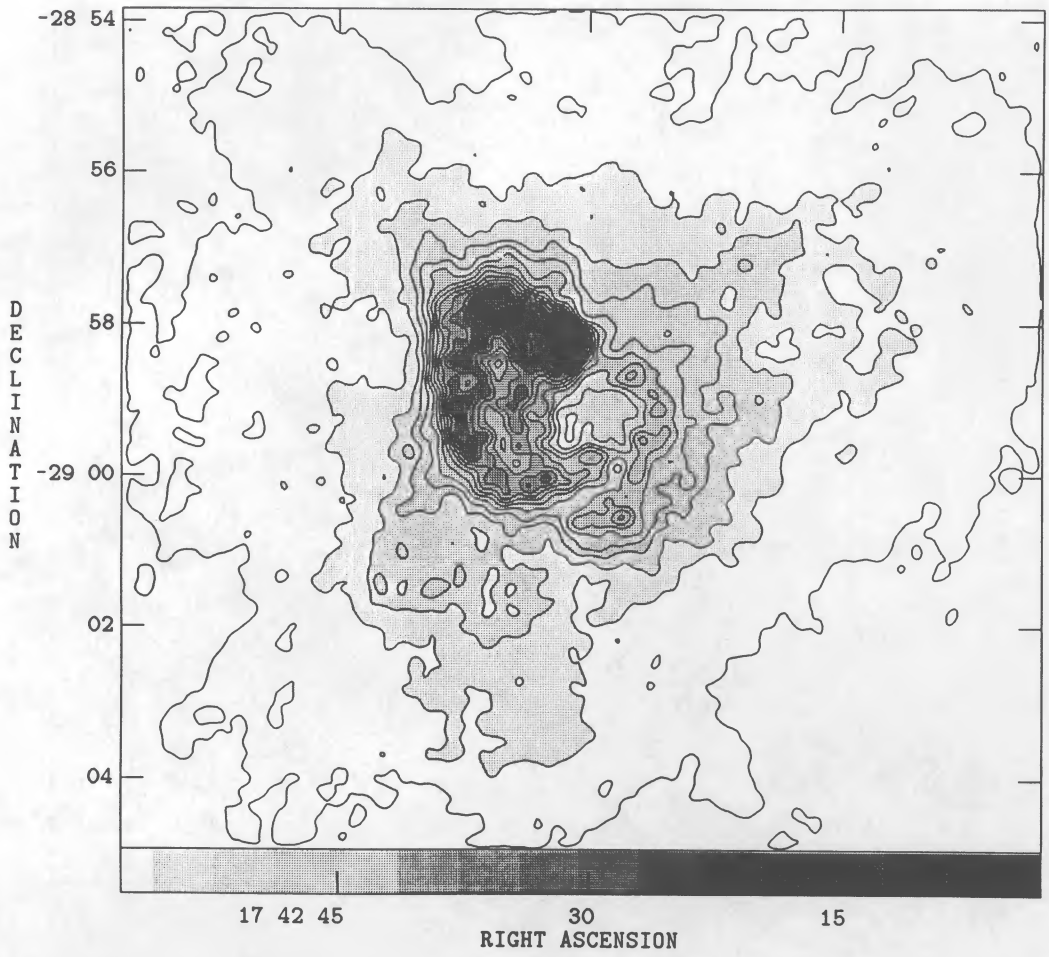

FIG. 5*a*

FIG. 5.—(*a*) The central part of Fig. 2 showing Sgr A and its halo at 90 cm. Contours are plotted at 100 mJy per beam intervals starting from 100 mJy per beam. (*b*) The same area of the 20 cm image convolved to the same resolution as the 332 MHz image (12″ × 12″). Contour intervals are 40 mJy per beam to 400 mJy per beam, and thereafter at 200 mJy per beam.

The Culgoora 92 cm image shows good structural agreement with the present data convolved to the same resolution. These data also show evidence of absorption by Sgr A West as pointed out by Yusef-Zadeh *et al.* (1986). The linear feature to the north, which they found is not obviously present in our data, and may represent partially resolved structure in the halo close to the base of one of the arched filaments. We detect weak emission (see Fig. 1) at the position of the elongated feature which Yusef-Zadeh *et al.* (1986) have discovered at 190 cm to the southeast of Sgr A. The 90 cm brightness temperature is ~ 1000 K which implies that the emission has a spectral index of $\alpha \sim -1$. This feature seems similar to other elongated structures in the Galactic plane, and we see no particular reason to consider it as evidence for a "radio jet" as suggested by Yusef-Zadeh *et al.* (1986).

b) The 20 Centimeter and 6 Centimeter Images

Although the 20 and 6 cm images are largely consistent with published data (e.g., Ekers *et al.* 1983; Lo and Claussen 1984; Yusef-Zadeh and Morris 1987), they represent a significant advance over previous high-resolution work, in that, they include more low-order spacings, and hence are more sensitive to extended structure, and give a more reliable spectral index distribution. Consequently, at 20 cm, the 7′ halo is well represented by these data. Although the halo has a complex structure, it appears to be a distinct component, particularly when convolved to a resolution of 12″ (Fig. 5*b*). The "Sgr A East halo" reported by Yusef-Zadeh and Morris (1987) appears to be a structural part of Sgr A East, and, unlike the "northwest streamers," does not appear to be a part of the 7′ halo. As can be seen in the 20 cm crosscut shown in Figure 7, the "Sgr A East halo" is evident as a distinct decrease in slope at 1 Jy per beam to the west, and 0.5 Jy per beam to the east. In fact the segment of the shell seen in the western part of Sgr A East at 90 cm is largely from the "Sgr A East halo" as defined by Yusef-Zadeh and Morris. This component cannot be accurately separated from Sgr A East, and hence we include this component in our flux density estimates of Sgr A East.

The shell of Sgr A East is well defined in both the 20 and 6 cm images and also shows a linear feature crossing the shell north-south at approximately $\alpha = 17^h42^m34^s$, which corresponds to a similar feature seen at 90 cm discussed above. This feature is clearly visible on the 90 and 20 cm crosscuts shown in Figure 7. The shape of the feature appears to follow the outline of Sgr A West, although it is offset to the east by $\sim 30''$ suggesting a possible interaction between Sgr A East and West.

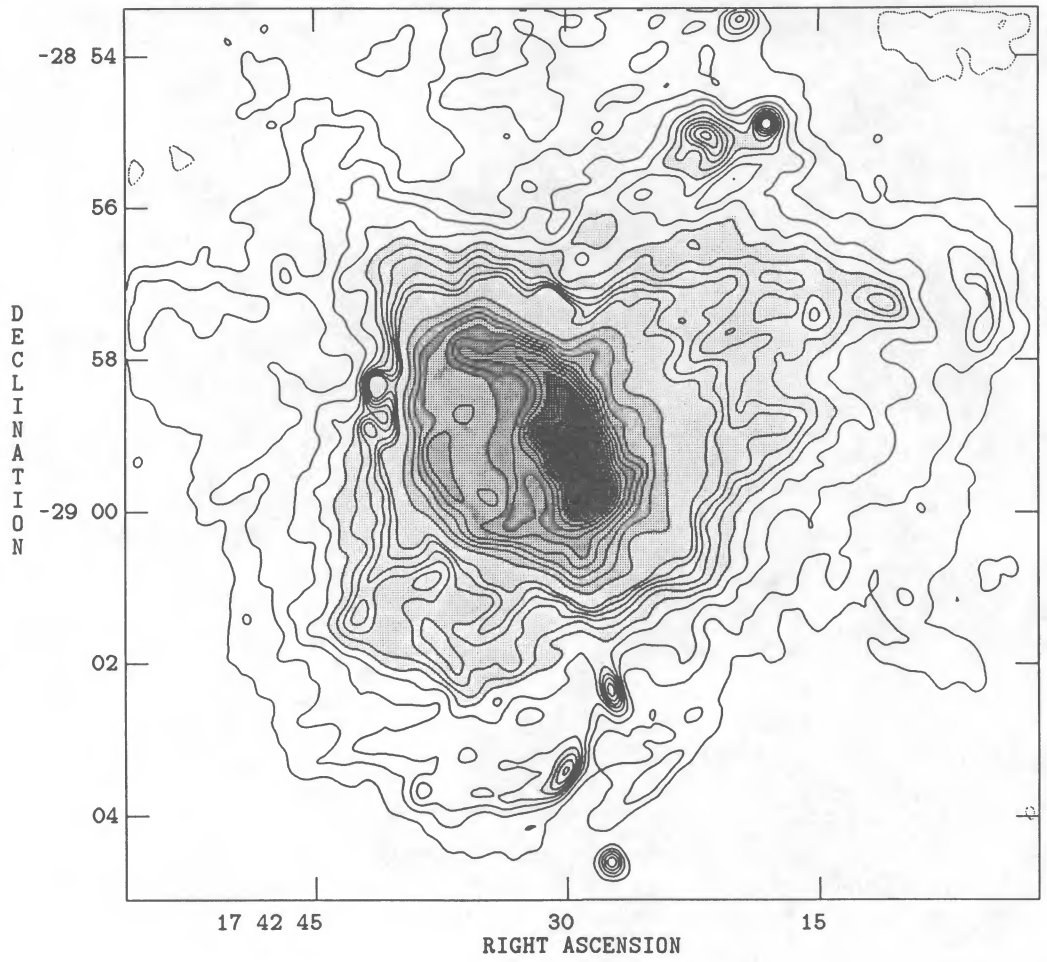

FIG. 5b

Although the 20 and 6 cm images of Sgr A West show similar overall structure, they differ considerably in detail. In particular the 6 cm western arc (the "arm" extending $\sim 1'$ to the south) appears wider and apparently displaced to the east in the 20 cm image. This effect must be due to the 20 cm thermal emission becoming optically thick, and absorbing both its own radiation and background nonthermal emission. At both frequencies considerable filamentary structure is present, which, although complex, appears to show a general elongation approximately perpendicular to the Galactic plane. This phenomenon is particularly striking (see also Killeen and Lo 1988) in the southern extension of the western arc and may indicate the presence of the strong poloidal magnetic field which has been proposed for the central region of our Galaxy (Yusef-Zadeh and Morris 1987).

The 20 cm brightness temperature of the Sgr A West emission rises to 20,000 K over a 10″ region $\sim 4''$ to the southwest of Sgr A*. Although this high brightness temperature could be due to the presence of a nonthermal component, it may also be consistent with thermal gas with high electron temperatures ($\geq$20,000 K) and significant 20 cm optical depth. High electron temperatures have also been deduced from this region from H76α measurements by van Gorkom, Schwarz, and Bregman (1985) and Schwarz, Bregman, and van Gorkom (1988).

c) *The Spectral Index Distributions*

A pseudocolor representation of the 20/90 spectral index distribution is shown in Figure 8*a* (Plate 14). This was derived directly from the images shown in Figure 5. Since these observations were not made using scaled arrays, the broad distribution of the derived spectral index could be affected, particularly toward the edge of the halo. As expected, the Sgr A West region is clearly present as a region of strongly positive ($\alpha > 0.5$) spectral index, as are a number of discrete H II regions in the field. The spectral index changes smoothly between Sgr A East and the adjacent halo and is almost flat ($\alpha \sim 0.0 \pm 0.2$), although there appears to be a decrease in α to ~ -0.5 toward the edge of the halo. As Sgr A East is known to be nonthermal (e.g., Ekers *et al.* 1983), it is clear that the apparent flat spectral index is due to the low-frequency turnover between 20 and 90 cm described by Mills and Drinkwater (1984). As the spectral index of Sgr A East is $\alpha \sim -1$ (see below), the 90 cm flux density can be extrapolated from the 20 cm value. Hence the observed 90 cm flux density is approximately 4 times smaller than the estimated. If this were due to a foreground absorbing medium, then an average optical depth of ~ 1.5 is required to give a flat 90/20 cm spectral index. The similarity between the 90/20 cm spectral index of Sgr A East and the adjacent halo

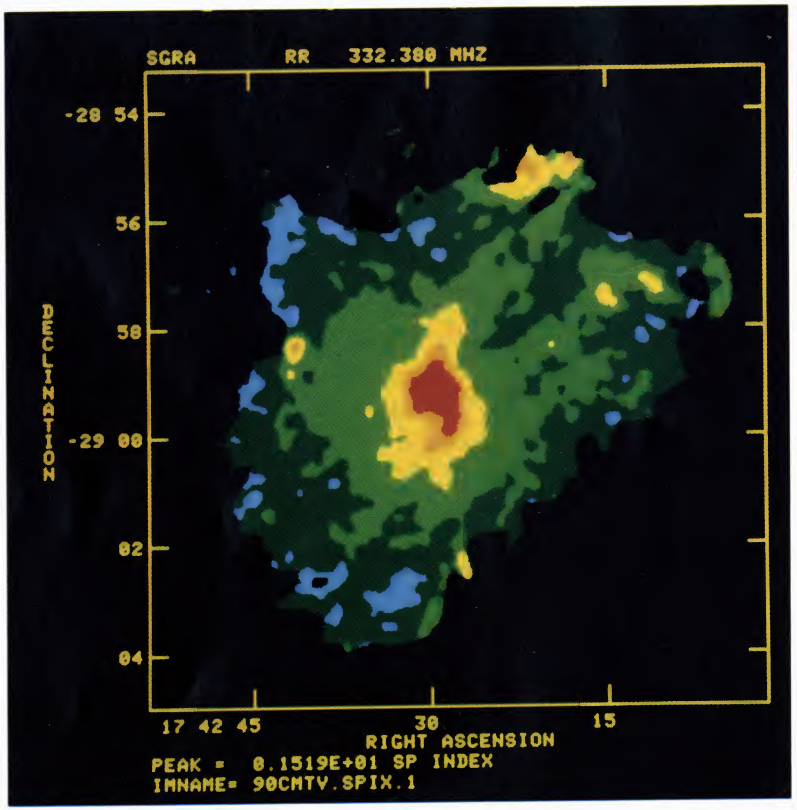

FIG. 8a

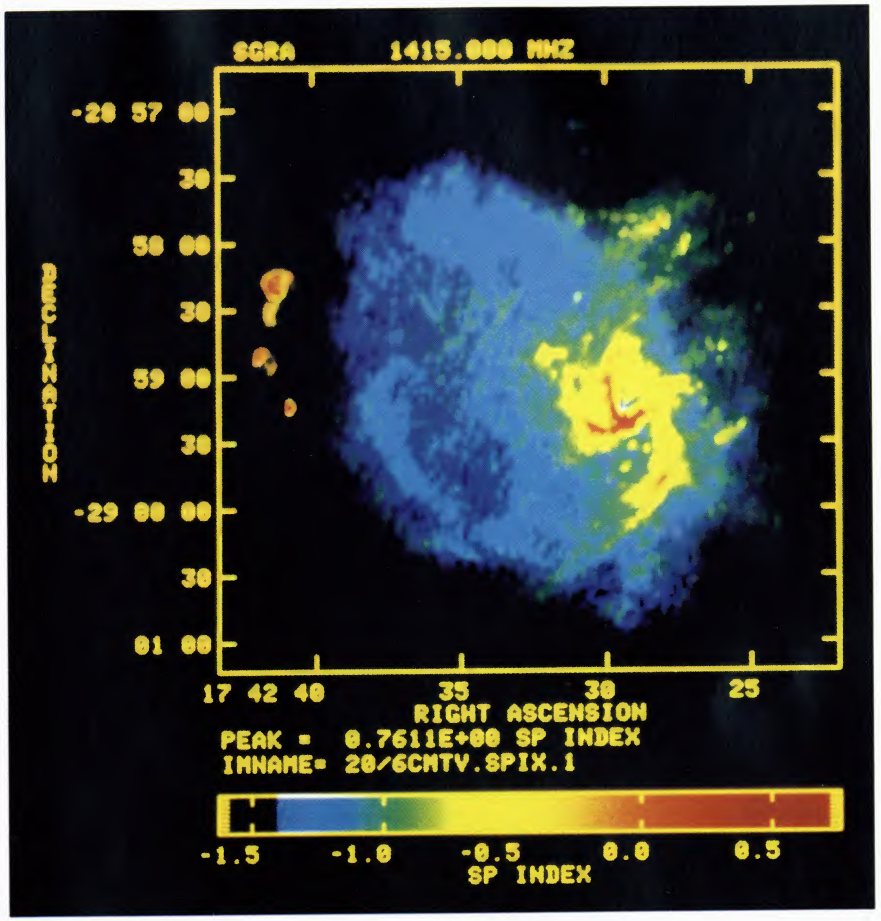

FIG. 8b

FIG. 8.—(*a*) A pseudocolor representation of the 20/90 spectral index distribution derived from the images shown in Fig. 5. (*b*) A pseudocolor representation of the 20/6 spectral index derived from the images shown in Figs. 3 and 4. The value of the spectral index corresponding to the different colors is shown by the color bar. In both images, the intensity is modulated by the brightness at the shorter wavelength.

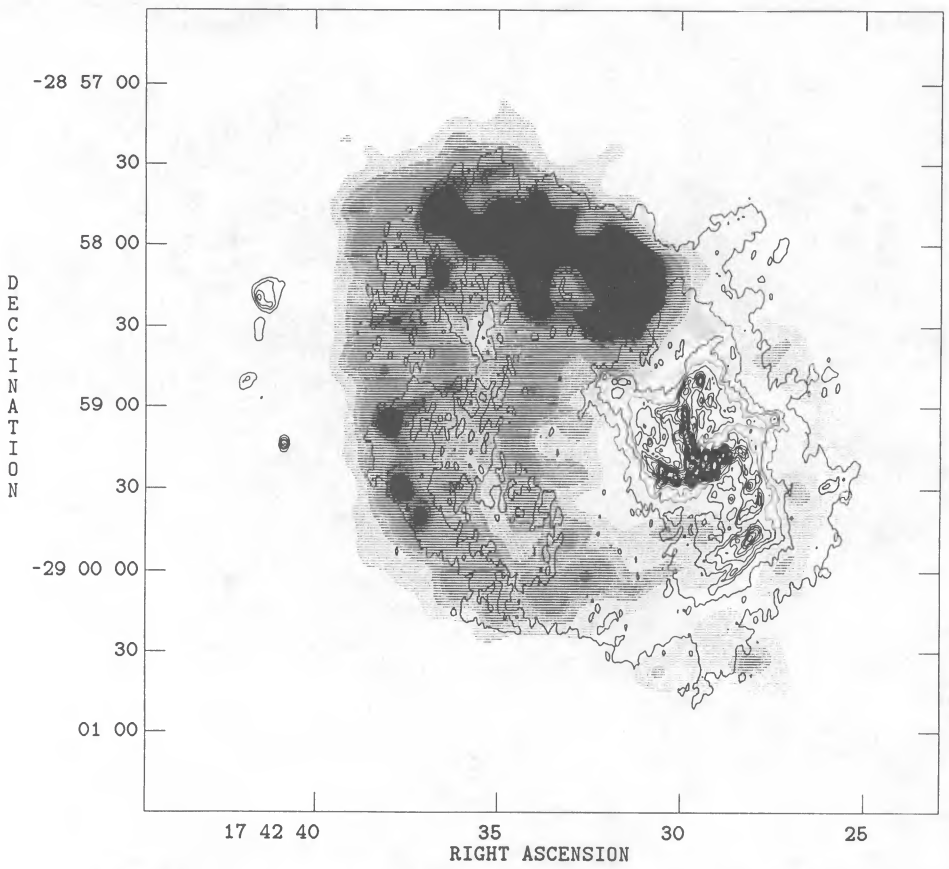

FIG. 6.—Gray scale of the 90 cm image (12″ × 12″ resolution) with the 6 cm image (1.″3 × 2.″5 resolution) superposed as contours. The contours are at 7 mJy per beam intervals until 175 mJy per beam, after which they are every 70 mJy.

suggests that this medium extends over several arcminutes (see, however, § IVc).

A pseudocolor representation of the 20/6 cm spectral index of Sgr A is shown in Figure 8*b*. This was derived from the images shown in Figures 3 and 4. The 20 cm image contains a contribution from the 7′ halo (~20 mJy per beam) which is not significantly present in the 6 cm image and will decrease the apparent 20/6 cm spectral index in regions of low brightness. We have estimated the missing flux density in the 6 cm image to be ~100 Jy by extrapolating from the measured visibilities at 20 cm. This is equivalent to a mean brightness of ~0.2 mJy per beam in Figure 3. The effect of this on the measured spectral index is small — <0.1% near the peak and ~5% near the lowest brightness areas. The spectral index image (Fig. 8*b*) shows clearly the thermal and nonthermal components in Sgr A. Both the chain of H II regions and Sgr A West show as regions of more positive spectral index. The spectral index of Sgr A West has an apparent value of −0.4 rather than −0.1, which is due to the presence of the nonthermal component of Sgr A East and the halo. The central parts of Sgr A West show a more positive spectral index, consistent with these regions being optically thick at 20 cm. Filaments with more positive spectral index, possibly thermal, appear to extend to the northwest, and may be associated with extensions to the northern arm, which the 90 cm measurements suggest cross the shell of Sgr A East. The spectral index of Sgr A East is typically ~ −1, somewhat more negative than the value estimated by Ekers *et al.* (1983). This offset is mainly due to the present observations including more extended emission, to which the earlier observations were not sensitive.

IV. DISCUSSION

a) Separating Components in the Sgr A Complex

When dealing with a region of the complexity of Sgr A, it is important to define the boundaries between individual components. Many lower resolution observations include all or part of the 7′ halo in determinations of the flux density of "Sgr A." This problem can result in significant errors when attempting to determine the spectrum of the source. One method of overcoming this problem is to measure the flux density within a series of radii (e.g., Reich *et al.* 1988). Using this method, however, it is difficult to assign flux densities to individual, nonconcentric components. While useful in dealing with single-dish observations, it is not well suited to synthesis observations which, because of missing zero spacings, lack sensitivity to extended structure. We have, therefore, adopted an approach of using both contour levels and crosscuts to define the extent of individual components and their respective zero levels.

In this paper we shall consider "Sgr A" to imply Sgr A*, Sgr A East and West only. The "Sgr A complex" consists of these three components together with the 7′ halo emission. We include the Sgr A East halo emission (Yusef-Zadeh and Morris 1987) as part of Sgr A East. In Figure 9 we show the 90, 20, and 6 cm images of the Sgr A area convolved to 12″. Inspection of a series of crosscuts (e.g., Fig. 7), suggests that the average bright-

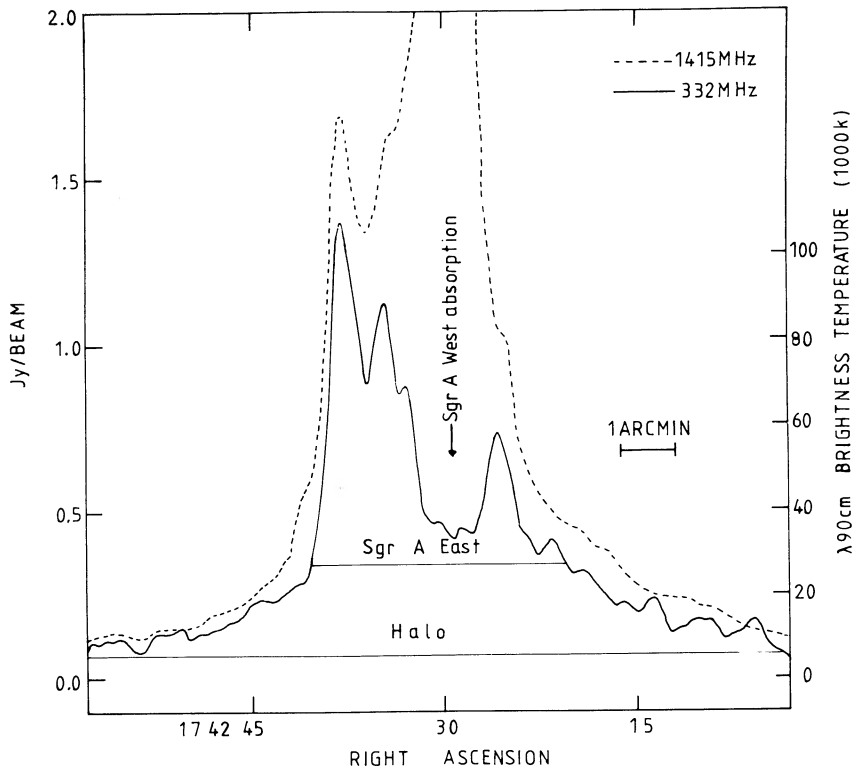

FIG. 7.—A typical crosscut at constant declination ($\delta = -28°59'6''$) at 90 cm and 20 cm (*dotted*) illustrating the absorption at the position of Sgr A West, and the halo emission. The horizontal lines show the assumed 90 cm base levels for Sgr A East and the halo.

ness of the halo at the position of Sgr A is $\approx 0.35 \pm 0.05$ Jy per beam at both 90 cm and 20 cm. Hence these offsets were removed from the images and the resulting flux densities of Sgr A and its halo are given in Table 2. At 6 cm the flux density of only Sgr A can be estimated, as the halo is not fully mapped due to lack of low order spacings.

Sgr A East and West cannot be separated using the above methods. In interpreting absorption in the 90 cm image, it would be useful to establish the structure of Sgr A East uncontaminated by Sgr A West. For this, the VLA 2 cm "D" array observation of Sgr A, described above, was used. At this wavelength, apart from the compact component Sgr A*, the emission is almost entirely thermal. Hence by assuming a constant electron temperature (T_e), it is possible to estimate the 2 cm optical depth ($\tau \sim 0.01$ if $T_e \sim 10{,}000$ K) across Sgr A West. As the free-free optical depth increases as $\lambda^{2.1}$, it can be readily evaluated for 6 cm and 20 cm. The brightness temperature expected for the thermal emission at these longer wavelengths is given by $T_b = T_e(1 - e^{-\tau})$. In Figure 9*d*, we show the "20 cm thermal emission" estimated in this way. In this case we have assumed $T_e = 5000$ K, although using $T_e = 10{,}000$ K has little effect on the results. The resulting image has been convolved to a resolution of 12″. The central 10″ of Sgr A West in this image is affected both by the compact source, and the possible presence of anomalously high electron temperatures (see § III*b*). A more serious problem is the lack of low-order spacings in the 2 cm image, which results in a lack of sensitivity to extended structure on scales greater than $\sim 2'$. In Figures 9*e* and 9*f*, we show the 20 cm and 6 cm images from which this thermal emission has been subtracted. The 20 cm nonthermal emission

TABLE 2

FLUX DENSITY MEASUREMENTS (Jy)

Wavelength (cm)	Sgr A	Sgr A Halo	Total	Sgr A East[a]	Reference
90	114 ± 20	256 ± 60	370 ± 50	...	This paper
20	240 ± 20	247 ± 35	487 ± 30	222 ± 20	This paper
6	88 ± 10	...	...	70 ± 10	This paper
	120	132	252	...	Mezger 1974
3	50	70	120	...	Pauls *et al.* 1976
0.6	40	42	82	...	Sofue *et al.* 1986

[a] After correcting for contribution from Sgr A West extrapolated from 2 cm flux density.

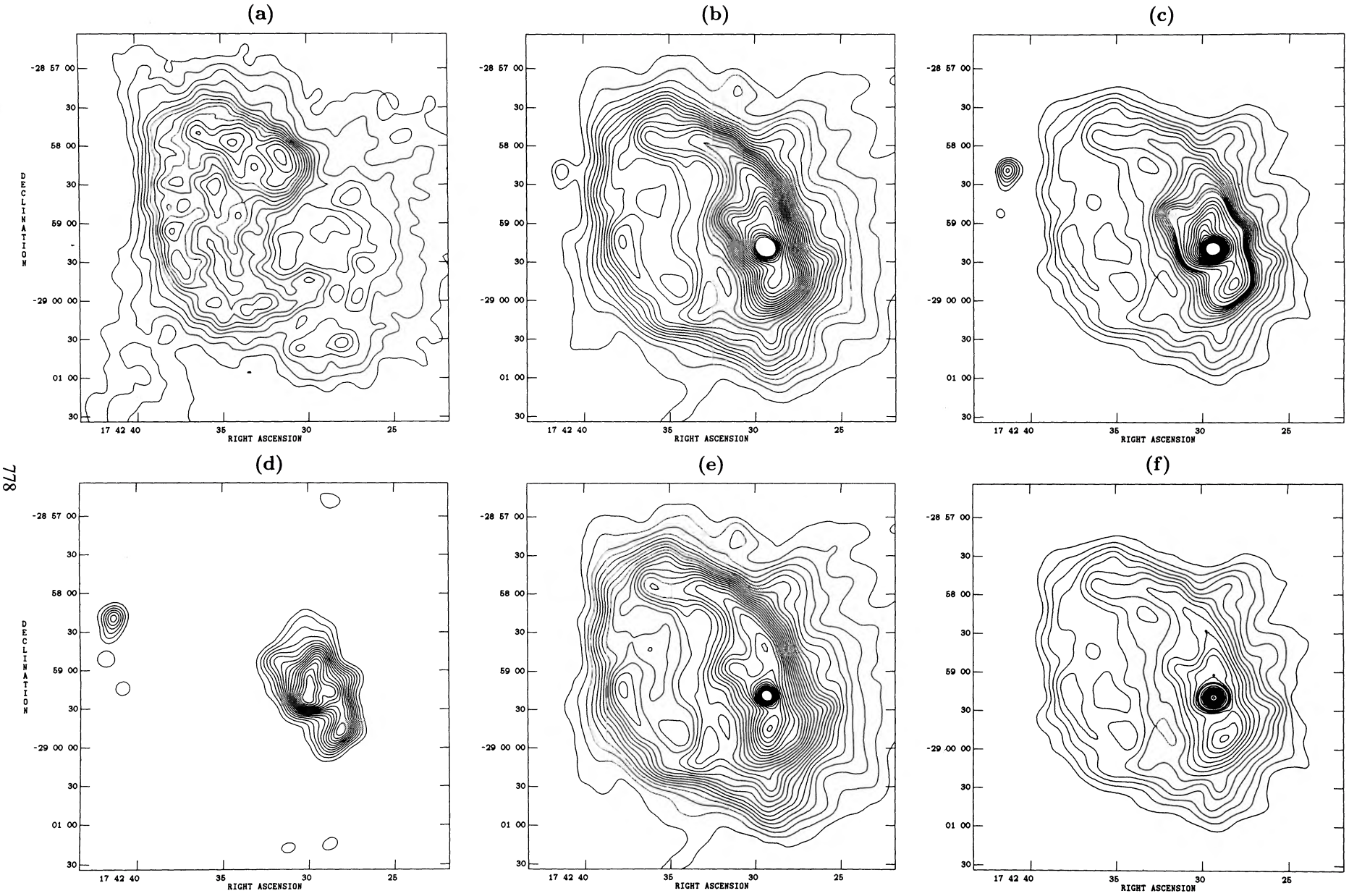

FIG. 9.—Images of the Sgr A region all convolved to the same 12″ × 12″ resolution. (*a*) 90 cm image; contour levels at intervals of 100 mJy per beam, starting from 350 mJy per beam. (*b*) 20 cm image; contour levels at intervals of 100 mJy per beam, starting from 350 mJy per beam. (*c*) 6 cm image; contour levels at intervals of 50 mJy per beam up to 800 mJy per beam, and then at 200 mJy per beam. (*d*) The derived 20 cm thermal emission (see text); contour levels 50 mJy per beam. (*e*) 20 cm image with estimated thermal emission subtracted. (*f*) 6 cm emission with estimated thermal emission subtracted.

was not corrected for the effect of absorption due to the thermal gas. The success of this method for removing small-scale structure can be judged from the fact that the eastern chain of H II regions are removed to an accuracy of a few percent. The 20/6 cm spectral index at the position of Sgr A West, deduced from Figures 9*e* and 9*f* is typically -0.9. This value is somewhat more positive than the rest of Sgr A East (~ -1.1), which is most likely caused by a residual weak extended thermal component to which the 2 cm measurements were not sensitive. From Mezger *et al.* (1988) we can estimate the total flux density of Sgr A West to be less than 30 Jy at 6 cm, and hence this extended component contributes, at most, 12 Jy. As this component is extended over 80″ × 60″ (Mezger and Wink 1986), its mean thermal contribution at 6 and 20 cm in our 12″ beam will be less than 0.3 Jy per beam.

The western part of the shell of Sgr A East clearly continues across the position of Sgr A West. It passes within ~10″ of the center of Sgr A West. This western part appears to be typically ~1 Jy per beam brighter than the average brightness of the rest of the shell at 20 cm, and as we have discussed above, less than 0.3 Jy per beam can be due to contamination by extended thermal emission. A nonthermal component appears ~30″ to the south of Sgr A*, and may be a continuation of the shell, a distinct component within Sgr A East or a nonthermal component associated with Sgr A West. The northern part of this component becomes contaminated by the effect of Sgr A*. The 20 cm flux density of this component is at least 5 Jy, and it may contribute to the diffuse component of Sgr A West discussed by Ekers *et al.* (1983).

b) Free-Free Absorption of Sgr A East by Thermal Gas

At 90 cm, ionized gas at a temperature of 5000 K, has an optical depth of unity if the emission measure is $\sim 10^5$ pc cm^{-6}. In § IV*a* we estimated the optical depth of the thermal gas in Sgr A West at 20 cm and, in fact, the lowest contour of Figure 9*d* (50 mJy per beam) corresponds to a 20 cm optical depth of 0.04. The optical depth varies as $\lambda^{2.1}$ and hence at 90 cm the same contour is equivalent to an optical depth of ~1. The approximate agreement between the area enclosed by this contour and the absorption feature seen at 90 cm (Fig. 9*a*) is clearly consistent with free-free absorption. It can be deduced from Figure 9*d* that most of Sgr A West has a 90 cm optical depth $\gg 1$ and hence will be effectively opaque to background radiation. The brightness temperature of the 90 cm image varies between 20,000 K and 40,000 K over the halo, rising to ~120,000 K in parts of the Sgr A East shell. As can be seen in Figure 7, at the position of Sgr A West, the brightness is depressed to ~30,000 K. Given the uncertainties in the halo structure, it is quite possible that at the position of Sgr A West, essentially all the radiation from Sgr A East has been absorbed. As the depth of the absorption feature is ~80,000 K, the only source in the field with sufficient brightness to create such a feature, is Sgr A East. Further, as can be seen in Figures 9*e* and 9*f* the shell of Sgr A East extends behind Sgr A West, providing a strong background against which absorption can occur. The average contribution from the broad galactic background, much of which may be missed by lack of low-order spacings, has been estimated by Anantharamaiah and Bhattacharya (1986) to be ~900 K, which can be neglected since the rms noise is ~1300 K.

The fact that the minimum of the absorption is close to, but not below, the mean level of the halo (see Figs. 5 and 7), suggests that most of the 90 cm halo emission is in front of Sgr A West. The brightness temperature at the position of Sgr A West is ~30,000 K, and extends over an area of at least 1 arcmin^2. The high electron temperatures discussed in § III*b* only occurs over a ~10″ region, and could only contribute marginally to this observed brightness temperature. In fact it is quite likely that at 90 cm, emission from this high-temperature region will be completely absorbed by lower temperature ionized gas in the thermal halo of Sgr A West. It appears, therefore, that much of the emission in the direction of Sgr A West must have a nonthermal origin. As the thermal component in most of Sgr A West is essentially opaque at 90 cm, the most likely source of this 90 cm nonthermal emission, given the approximate agreement in brightness temperatures, is the 7′ halo. We will discuss this further in § IV*e*.

A more quantitative estimate of the absorption across Sgr A was attempted by using the 20 and 6 cm images from which the thermal emission has been removed (Figs. 9*e* and 9*f*) to estimate the spectral index for each pixel between these two wavelengths. This can then be used to linearly extrapolate the 20 cm brightness to 90 cm. This method was possible only for Sgr A as the 6 cm halo emission was not well defined, and hence estimates of the halo contribution (0.35 Jy per beam; see § IV*a*) were subtracted from the 20 and 90 cm images before the calculation. The observed and extrapolated 90 cm intensities were then combined to give a crude estimate of the 90 cm optical depth, τ, across Sgr A. The optical depth is calculated by assuming that the absorbing medium is completely in front of the 90 cm emission, which is then attenuated by $e^{-\tau}$. Small errors in the estimated base level become very significant as the optical depth becomes large, and values of τ higher than 4 must be treated as lower limits, and the smaller values of τ have uncertainties ± 0.5. The optical depth distribution derived in this way is shown in Figure 10.

As expected, most of the Sgr A West region shows high optical depth ($\tau > 4$), implying an emission measure of at least 5×10^5 pc cm^{-6}. This distribution is superposed on an extended background optical depth of ~1–2, which corresponds to an extended thermal component undetected by the 2 cm measurements. The region with optical depth ($\tau > 3$) appears to be larger than the 6 cm image of Sgr A West, and implies that the thermal "spiral" is embedded in a halo of ionized gas with an emission measure of $\sim 2 \times 10^5$ pc cm^{-6} and an extent of 1.′5. This halo can be tentatively identified with the 80″ × 60″ component observed by Mezger and Wink (1986) at 1.3 cm and 9 mm and designated by them as Sgr A West (extended). Using a simple, uniform density ($N_e \sim 200$ cm^{-2}) spherical model for the ionized gas (Mezger and Henderson 1967) we estimate this component to contain $\sim 500\ M_\odot$ of ionized gas. This component would have a flux density of ~3 Jy at 6 cm and 20 cm and may, together with the ~5 Jy nonthermal component discussed in § IV*a*, be part of the diffuse component of Sgr A West referred to by Ekers *et al.* (1983).

The north and south "spiral arms" of Sgr A West are clearly visible (Fig. 5*a*) where they cross the shell of Sgr A East and can be traced further than is evident in emission on the 6 cm contour image shown in Figure 4, although this extension is faintly visible on the 6 cm gray scale plots of Yusef-Zadeh and Morris (1987). Using crosscuts we estimate the increase in optical depth at the positions of the arms to be ~1, indicating an emission measure of $\sim 10^5$ pc cm^{-6}. The 90 cm brightness temperatures at the position of the spiral features are ~40,000 K, although as the 12″ beam does not fully resolve these, they

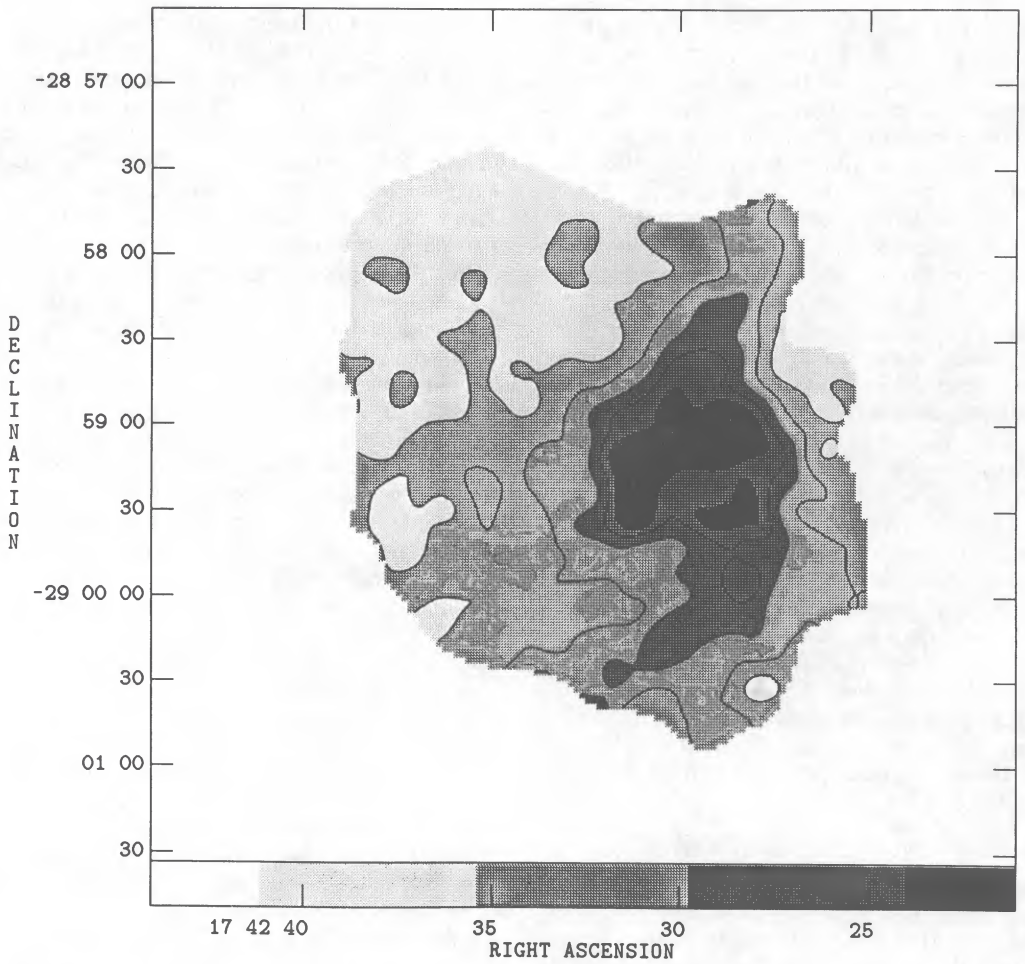

FIG. 10.—The "optical depth" distribution across Sgr A East derived in the manner described in the text. Contour levels shown are 1.5, 2.0, 2.5, 3.0, and 3.5. Typical errors are ± 0.5.

should be considered upper limits, and the corresponding optical depths and emission measures, lower limits.

There is no evidence that either of these features are seen in absorption against the $\sim 7'$ halo at 90 cm. Unless the arms terminate shortly after crossing the shell of Sgr A East, then Sgr A West cannot be in front of the halo, otherwise an optical depth of 0.5 would be detectable against the halo. The 20/6 cm spectral index image shown in Figure 8*b* suggests that thermal emission, possibly associated with a continuation of the northern arm of Sgr A West, is present to the northwest and yet does not show up as absorption against the halo. This observation might seem to suggest that this gas is toward the far side of the halo; however, see the discussion in § IV*e*.

Apart from Sgr A West and its arms, the optical depth distribution across the rest of Sgr A East shows no strong variations. Most of the source shows an optical depth between 1 and 2, with the higher values in the southern part of the shell. This distribution could be due to a foreground H II region with an emission measure of $\sim 10^5$ pc cm^{-6}, or as discussed in the following section, may be associated with the thermal component in the $\sim 7'$ halo.

c) The Halo Emission

It is clear from Figures 1 and 5 that a distinct halo surrounds Sgr A East and West. We shall therefore attempt to separate its properties from the other components. The flux density and spectral index of the $\sim 7'$ halo are difficult to determine. At 7 mm (43 GHz) the halo flux density, within a 6′ radius, appears to be ~ 42 Jy (Sofue *et al.* 1986), which increases to 132 Jy at 6 cm (Mezger 1974). We estimate the 20 cm flux density (above the 50 mJy per beam contour) to be 247 ± 35 Jy. Our estimate of the flux density for Sgr A East and West of 240 Jy (above the 0.35 Jy per beam contour) is significantly higher than that of Yusef-Zadeh and Morris (1987) due to the inclusion of Sgr A East halo in the flux density of Sgr A East. Pauls *et al.* (1976) give the combined flux density of Sgr A and the halo at 3 cm (10 GHz) to be 120 Jy. Our 2 cm measurements, together with those of Ekers *et al.* (1983) and Brown and Liszt (1984), constrain the 3 cm flux density of Sgr A West to be ~ 20 Jy. The contribution from Sgr A East at 3 cm can be estimated to be ~ 30 Jy by extrapolation from our 6 cm flux density ($\alpha \sim -1$). Hence we assume a halo flux at 3 cm of ~ 70 Jy. Although the 190 cm (160 MHz) observations of Dulk and Slee (1974) do not separate the halo flux from Sgr A, the emission is extended over 7′ and hence the observed 114 Jy must be mainly from the halo rather than Sgr A. These estimates for the flux density of the halo given in Table 2 and are shown in Figure 11.

These flux densities indicate that, at centimeter wavelengths, the halo has a relatively steep spectral index ($\alpha \sim -0.7$), implying that the emission is mainly nonthermal. If we extrapolate

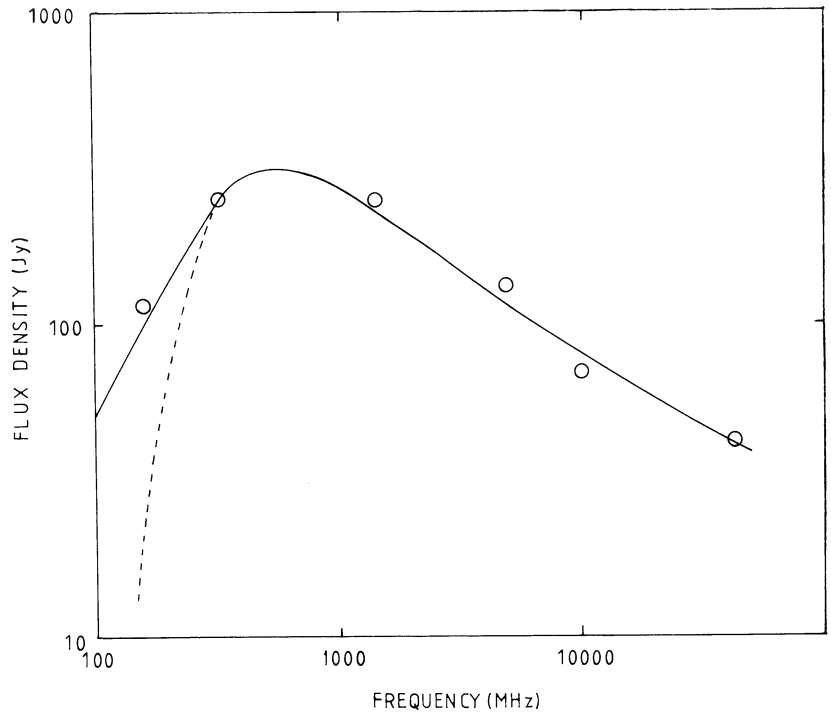

FIG. 11.—The spectrum of the halo surrounding Sgr A, from which our estimates of the flux density of Sgr A has been removed. The solid line shows a model of uniformly mixed thermal and nonthermal emission for the halo described in the text. The dashed line shows the effect of absorption by a foreground H II region with the required optical depth to account for the 90 cm flux density.

the 20 cm flux density to 90 cm, then we could expect a value of ~ 700 Jy, whereas we measure 256 ± 60 Jy. Thus it appears that an optical depth of order unity at 90 cm is required to produce this turnover. As we have suggested above for Sgr A East, this turnover could be caused by free-free absorption by a conventional, foreground H II region, extended over $\sim 7'$ with an emission measure of 10^5 pc cm^{-6}. However, such an H II region would have an optical depth of at least 4 at 190 cm which would produce a much steeper cutoff as is shown by the dashed line in Figure 11. The spectral index between 90 and 190 cm can be reduced, if we assume the thermal and nonthermal components to be uniformly mixed. For the simplest such model,

$$S \sim (S_{\rm nt}\, \nu^{\alpha} + S_{\rm th})\left(\frac{1 - e^{-\tau}}{\tau}\right)$$

(e.g., Gregory and Seaquist 1974), where $S_{\rm nt}$ and $S_{\rm th}$ are the nonthermal and thermal flux densities, and τ is the free-free optical depth at frequency, ν. In Figure 11, we show an example of the above model compared with the observed flux density of the halo, in which we have assumed $E = 2.7 \times 10^5$ pc cm^{-6}, $T_e = 5000$ K, and that $\alpha = -0.7$. $S_{\rm th}$ can be estimated in terms of the emission measure, electron temperature and size of the emitting region. We assume a half-power size for the thermal gas of $4' \times 4'$ which gives the mass of thermal gas in this halo component, assuming a filling factor of unity, to be $\sim 3 \times 10^3\, M_{\odot}$.

The electron temperature can be varied between 5000 and 10,000 K, although an increase in electron temperature also requires an increase in emission measure. Nevertheless the thermal component in the halo must have an optical depth of ~ 2 at 90 cm. This value is similar to the 90 cm optical depth measured across the shell of Sgr A East, and, since it appears plausible that the thermal component of the halo is responsible for this, implies that Sgr A East be on the far side of the halo. It may be possible to detect radio recombination lines from the thermal gas in the halo, particularly in front of Sgr A East where stimulated emission is possible. Such a detection would also provide a measurement of the radial velocity of the halo.

Although the large-scale structure of the 90 cm and 20 cm halos are similar, there is little correspondence between individual structures. The possible shell structure at 90 cm to the SE of Sgr A can be associated with a similar feature at 20 cm, and may be evidence for a supernova remnant associated with the "wisp" (feature E) as suggested by Ho *et al.* (1985). The "wisp" itself, together with the features F and G reported by Ho *et al.* are not detected in the 90 cm data. The "wisp" and feature F show polarization and hence must be nonthermal. If we extrapolate the 20 cm flux density of the wisp to 90 cm we obtain ~ 2 Jy which should be detectable. Its apparent 90/20 cm spectral index (Fig. 8*a*) is close to zero which may imply that it has a low-frequency turnover similar to Sgr A East. It could be that many of the components seen in the direction of the halo at 20 cm are attenuated by the free-free absorption of the thermal gas in the halo at 90 cm.

There is, however, a decrease of ~ 100 mJy per beam in brightness at the position of the cluster of H II regions (A, B, C, D of Ekers *et al.*) to the east of Sgr A East. This decrease is not surprising, as Ekers *et al.* showed the central emission measures to be in excess of 10^6 pc cm^{-6}. It could suggest that these

H II regions are in front of a significant fraction of the halo emission. However, the depression in the 90 cm brightness temperature extends over several beam areas and is elongated roughly in PA 70°. The H II region cluster is too compact to account for all this extended absorption, which may be due an outer low-density envelope with an emission measure of $\sim 10^5$ pc cm^{-6}. The 84 GHz image of Salter *et al.* (1988) shows a feature elongated in the same position angle as the 90 cm absorption, which we also estimate to have an emission measure of 1.5×10^5 pc cm^{-6}. It must be pointed out, however, that the 20 cm emission is also depressed in this region (Fig. 5), which may indicate that the depression at 90 cm could be due to an absence of emission, rather than absorption.

Using equipartition assumptions (Miley 1980), and that the ratio of relativistic protons to electrons is 100, we can estimate the parameters of the relativistic particles and magnetic fields in the halo component. Hence, the total energy in relativistic particles in this component is about 5×10^{50} ergs which is comparable to that of Sgr A East ($\sim 2 \times 10^{50}$ ergs). The pressure of the relativistic particles in the halo is an order of magnitude lower than the pressure estimated for Sgr A East.

d) The Compact Source and Interstellar Scattering

Molecular absorption measurements (Whiteoak, Gardner, and Pankonin 1983) have suggested that Sgr A* may be in front of Sgr A West, which would enable it to avoid attenuation by this source. However, because of the patchiness in the molecular distribution, such arguments may not be conclusive (Liszt *et al.* 1983). The 6 cm measurements show Sgr A* to be offset $\sim 4''$ to the north of the highest emission measure regions of Sgr A West. At 90 cm, extrapolating the results of Davies, Walsh, and Booth (1976), we would expect its diameter due to scatter broadening to be 13″, and hence should have a width of $\sim 16''$ when measured with the 12″ beam. At the position of Sgr A* we find no compact source stronger than 100 mJy which is consistent with the limit set by Davies, Walsh, and Booth (1976) at 75 cm. If the intrinsic spectrum of the source shows no low-frequency cutoff, then this would be consistent with it being absorbed by free-free emission with an optical depth > 2.5. As can be seen from Figure 10, the area of high optical depth is extended over 1′ and clearly could include Sgr A*. We, therefore, conclude that Sgr A* is either embedded in or behind the ionized gas associated with Sgr A West, as suggested by Liszt *et al.* (1983). Thus, it is possible that much of the scatter broadening of this source may occur in the ionized gas associated with Sgr A West.

e) The Structure of the Sgr A Complex

There seems little doubt that Sgr A West and Sgr A* are situated close to or at the Galactic center. The current observations show conclusively that Sgr A East is on the far side of the center, although from other constraints (e.g., Güsten and Downes 1980) it must still be within 100 pc of the nucleus. It is also interesting to note that, after removing the thermal emission, the brightest part of the shell of Sgr A East is at the position of Sgr A West, indicating that the two components are physically related. This possibility is also suggested by the similarity between the shape of the linear N-S feature and the boundary of the ionized gas associated with Sgr A West, which is discussed in § III*b*. The N-S feature and the western edges of Sgr A East and Sgr A West coincide with enhanced molecular emission in the cirumnuclear disk (Güsten 1986) as if both components were colliding with the same molecular clouds; a possible physical association is suggested. It appears that Sgr A East is situated toward the far side of the halo if we are to account for its 90 cm turnover by free-free absorption by the thermal component in the halo.

In § IV*b*, we noted possible evidence that the 90 cm halo emission was also situated in front of the thermal gas associated with Sgr A West. This assertion was based on two pieces of evidence: (1) the brightness temperature of the absorption feature at the position of Sgr A West agrees closely with the brightness temperature of the halo, and (2) extensions to the thermal arms associated with Sgr A West showed up strongly in absorption ($\tau \sim 1$) against the shell of Sgr A East, and yet cannot be detected against the halo. At first sight, this appears to be evidence that the halo is mostly in front of Sgr A West. However, the thermal/nonthermal model we have proposed for the halo, while not ruling out this possibility, also provides a natural explanation for these observations. Because the halo thermal component has a significant optical depth at $\lambda 90$ cm, most of the nonthermal emission we detect must come from the near side of the halo. Thus failure to detect absorption of the halo by the thermal gas associated with Sgr A West, whilst ruling out the possibility that Sgr A West is towards the near side of the halo, cannot be used as decisive evidence that Sgr A West is behind the halo.

In Figure 12*a* we show a possible configuration of the components within Sgr A, where Sgr A West has beeen assumed to be at the center of the halo. It has been suggested (e.g., Yusef-Zadeh and Morris 1987) that the halo is a secondary manifestation of the supernova explosion which produced Sgr A East and may represent leakage of cosmic ray electrons throughout the shell of Sgr A East. If our deduction from optical depth considerations (§ IV*a*) that the halo is largely in front of Sgr A East is correct, then such leakage must be preferentially on the near side of Sgr A East. Such a configuration may be a consequence of Sgr A East being bounded by giant molecular clouds on the far side, as suggested by Goss *et al.* (1985) and Mezger *et al.* (1988). If Sgr A East is embedded within the halo, then Sgr A West must be situated close to the center of the halo not only in the plane of the sky (see Fig. 8*a*), but also in the line of sight. We could then speculate that the relativistic electrons originate in Sgr A* and diffuse into the halo.

An alternative configuration for the Sgr A complex is shown in Figure 12*b*, as our data cannot rule out the possibility that the halo is a spatially separate component, which may be in front of both Sgr A East and West. If we consider the halo as a separate object, then its nonthermal spectrum, together with its relativistic energy of 5×10^{50} ergs and size of ~ 20 pc could suggest that it was an evolved supernova remnant, of which Sgr A East may be either a younger example, or one which has occurred in a much denser environment (Goss *et al.* 1983; Ekers *et al.* 1983). Several other components of the Sgr A complex could possibly be supernova remnants such as the ring to the southeast. It should be pointed out, however, that there are many structures which are unique to the Galactic center, such as the threads. Although there is little evidence of shell-type structures in the halo, such ordered structures might be expected to be disrupted by the violent environment close to the Galactic center, once the pressure within the remnant is roughly equal to the ambient pressure. The displacement of the center of Sgr A East from Sgr A West could suggest that the structure is elongated at an angle of 10° to 20° from the line of sight from the Galactic center to the Sun.

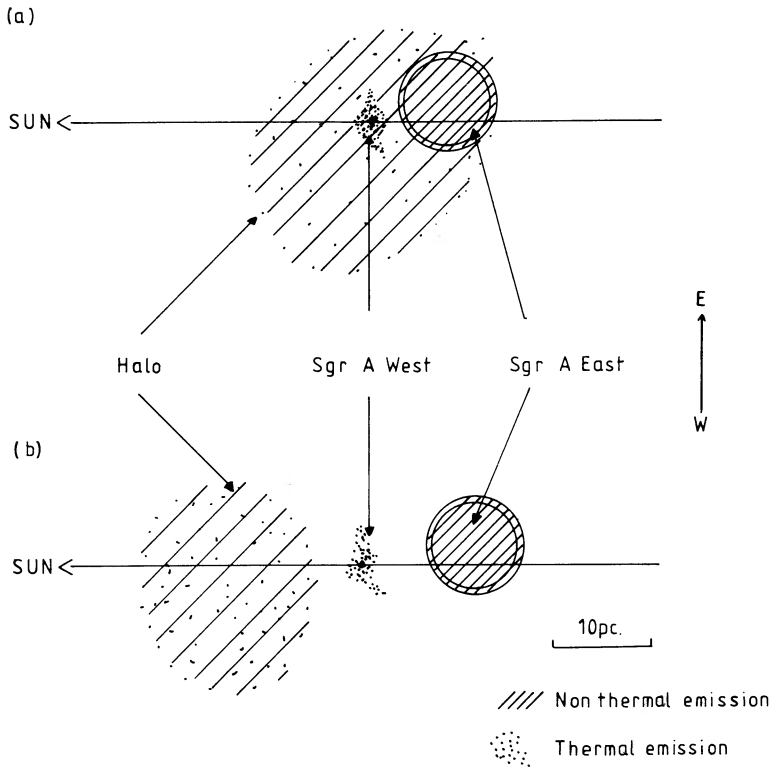

FIG. 12.—Two possible configurations for the structure of radio emission in the Sgr A complex. As discussed in the text our observations demonstrate conclusively that Sgr A East is behind Sgr A West, and there are strong indications that Sgr A East is to the far side of the halo. The overall elongation of the structure is not constrained by our measurements: the three components could be in close contact as in (*a*) or well separated as in (*b*). The offset of $\sim 1'$ between the centers of Sgr A East and West may be produced by inclining the above structures to the line of sight.

Supernova explosions would be a natural consequence of the ongoing star formation at the Galactic center. However, a somewhat more speculative possibility is that Sgr A East and the halo are two nonthermal components which have originated from the active nucleus. This would then suggest similarities with Seyfert-type activity in the nuclei of spiral galaxies, which is thought to originate in a central engine. Many of these have associated radio emission which appears to originate in collimated ejection from the nucleus, and rarely seems to align with the rotation axis of the spiral (e.g., Booler, Pedlar, and Davies 1982). Evidence for such collimated ejection is seen in the compact, nonthermal radio components which straddle the optical nucleus (Ulvestad and Wilson 1984; Unger *et al.* 1986). The origin of these components is unclear as their energy in relativistic particles/magnetic fields range from 10^{51} to 10^{55} ergs. These high energies and their collimation would appear to rule out conventional SNRs. This type of phenomena also occurs in normal spirals such as M51 (Ford *et al.* 1985), although this can often only be detected with the highest available sensitivity. The lower limit of $\sim 10^{51}$ ergs for these components (Unger *et al.* 1986) is largely due to instrumental sensitivity and an object such as Sgr A East or the halo would be undetectable, if situated in a galactic nucleus beyond a few Mpc. It is of interest to note that, if Sgr A East were to be the remnant of a supernova which had exploded directly into a giant molecular cloud, then an event of at least 4×10^{52} ergs in total energy would be required to produce the observed radio emission, although this can be reduced if the supernova progenitor excavates a cavity with a strong stellar wind (Mezger *et al.* 1988).

At this stage it is unclear to us whether Sgr A East represents the high-energy end of a distribution of SNR, or one of the lower energy examples of the class of radio components which appear common in the active nuclei of spiral galaxies.

V. CONCLUSIONS

1. At 90 cm, Sgr A West is seen in absorption against Sgr A East, showing that the latter is definitely on the far side of the former.

2. The 90 cm absorption region is more extensive than the thermal emission seen in high-frequency images and implies that Sgr A West is embedded in a thermal halo approximately 5 pc in diameter containing $\sim 500\ M_\odot$ of ionized gas.

3. Both the north and south "spiral arms" associated with Sgr A West are seen in absorption at 90 cm against the shell of Sgr A East indicating an optical depth of ~ 1, although not against the adjacent halo.

4. The parts of Sgr A East which are not already absorbed by Sgr A West at 90 cm, show evidence of a low-frequency turnover consistent with free-free absorption by ionized gas extended over at least 8 pc with an optical depth of ~ 1.5–2.

5. The $\sim 7'$ halo appears to be a separate component with a

spectral index of -0.7 and energy in relativistic particles of 5×10^{50} ergs. It also shows a low-frequency turnover which is consistent with a mixture of thermal and nonthermal components within the halo. The thermal component seems also to be responsible for at least part of the low-frequency turnover of Sgr A East. We estimate this gas to have an emission measure of $\sim 3 \times 10^5$ pc cm^{-6} if $T_e = 5000$ K.

6. We do not detect the compact radio source Sgr A* at 90 cm, implying that the source is embedded in or behind Sgr A West. In either case the high degree of scatter broadening in this source may be occurring in the ionized gas associated with Sgr A West.

We wish to thank Durga Bagri and Rick Perley for assistance with the 90 cm observations. We thank Chris Salter, Farhad Yusef-Zaden, D. J. Saikia, Ko Hummel, and Neil Killeen for useful discussions. A. P. wishes to acknowledge the hospitality of the VLA staff. The National Radio Astronomy Observatory is operated by Associated Universities Inc., under cooperative agreement with the National Science Foundation.

REFERENCES

Anantharamaiah, K. R., and Bhattacharya, D. 1986, *J. Ap. Astr.*, **7**, 141.
Balick, B., and Brown, R. L. 1974, *Ap. J.*, **194**, 265.
Booler, R. V., Pedlar, A., and Davies, R. D. 1982, *M.N.R.A.S.*, **199**, 229.
Brown, R. L., and Liszt, H. S. 1984, *Ann. Rev. Astr. Ap.*, **22**, 223.
Cornwell, T. 1985, in *Synthesis Imaging*, ed. R. A. Perley, F. R. Schwab, and A. H. Bridle (Green Bank: NRAO), p. 137.
Cotton, W. D. 1985, in *Synthesis Imaging*, ed. R. A. Perley, F. R. Schwab, and A. H. Bridle (Green Bank: NRAO), p. 123.
Davies, R. D., Walsh, D., and Booth, R. S. 1976, *M.N.R.A.S.*, **177**, 319.
Dulk, G. A., and Slee, O. B. 1974, *Nature*, **248**, 73.
Ekers, R. D., van Gorkom, J. H., Schwarz, U. J., and Goss, W. M. 1983, *Astr. Ap.*, **122**, 143.
Ford, H. C., Crane, P. C., Jacoby, G. H., Lawrie, D. G., and van der Hulst, J. M. 1985, *Ap. J.*, **293**, 132.
Gopal-Krishna, S. G., Sarma, N. V. G., and Joshi, M. N. 1972, *Nature*, **239**, 91.
Goss, W. M., Schwarz, U. J., Ekers, R. D., and van Gorkom, J. H. 1983, in *IAU Symposium 101, Supernova Remnants and Their X-Ray Emission*, ed. J. Danziger and P. Gorenstein (Dordrecht: Reidel), p. 65.
Goss, W. M., Schwarz, U. J., van Gorkom, J. H., and Ekers, R. D. 1985, *M.N.R.A.S.*, **215**, 69P.
Gregory, P. C., and Seaquist, E. R. 1974, *Ap. J.*, **194**, 751.
Güsten, R. 1986, in *The Galactic Center*, ed. D. C. Backer (AIP Conf. Proc. 155) (New York: AIP), p. 19.
Güsten, R., and Downes, D. 1980, *Astr. Ap.*, **87**, 6.
Ho, P. T. P., Jackson, J. M., Barrett, A. H., and Armstrong, J. T. 1985, *Ap. J.*, **288**, 575.
Killeen, N., and Lo, K. Y. 1988, in *IAU Symposium 136, The Galactic Center*, ed. M. Morris (Dordrecht: Reidel), in press.
LaRosa, T. N., and Kassim, N. E. 1985, *Ap. J. (Letters)*, **299**, L13.
Liszt, H. S., van der Hulst, J. M., Burton, W. B., and Ondrechen, M. P. 1983, *Astr. Ap.*, **126**, 341.
Little, A. G. 1974, in *IAU Symposium 60, Galactic Radio Astronomy*, ed. F. J. Kerr and S. C. Simonson III (Dordrecht: Reidel), p. 491.
Lo, K. Y., and Claussen, M. J. 1984, *Nature*, **306**, 647.
Mezger, P. G. 1974, in *Proc. ESO/SRC/CERN Conference on Research Programmes for Large Telescopes*, ed. A. Reiz (Munich: ESO), p. 79.
Mezger, P. G., and Henderson, A. P. 1967, *Ap. J.*, **147**, 471.
Mezger, P. G., and Wink, J. E. 1986, *Astr. Ap.*, **157**, 252.
Mezger, P. G., Zylka, R., Salter, C. J., Wink, J. E., Chini, R., and Kreysa, E. 1988, *Astr. Ap.*, submitted.
Miley, G. 1980, *Ann. Rev. Astr. Ap.*, **18**, 165.
Mills, B. Y., and Drinkwater, M. J. 1984, *J. Ap. Astr.*, **5**, 43.
Morris, M., and Yusef-Zadeh, F. 1985, *A.J.*, **90**, 2511.
Oort, J. H. 1985, in *The Milky Way Galaxy*, ed. H. van Woerden, R. J. Allen, and W. B. Burton (Dordrecht: Reidel), p. 349.
Pauls, T., Downes, D., Mezger, P. G., and Churchwell, E. 1976, *Astr. Ap.*, **46**, 407.
Pedlar, A., Davies, R. D., Hart, L., and Shaver, P. A. 1978, *M.N.R.A.S.*, **182**, 473.
Perley, R. 1988, in *Synthesis Imaging*, ed. R. A. Perley, F. R. Schwab, and A. H. Bridle (San Francisco: Astronomical Society of the Pacific), in press.
Reich, W., Sofue, Y., Wielebinski, R., and Seiradakis, J. H. 1988, *Astr. Ap.*, **191**, 303.
Rots, A. H. 1985, in *Synthesis Imaging*, ed. R. A. Perley, F. R. Schwab (Green Bank: NRAO), p. 231.
Salter, C. J., Sinha, R. P., Stobie, E. B., Kerr, F. J., and Hobbs, R. W. 1988, *M.N.R.A.S.*, **232**, 407.
Schwarz, U. J., Bregman, J. D., and van Gorkom, J. H. 1988, *Astr. Ap.*, in press.
Sofue, Y., Inoue, M., Handa, T., Tsuboi, M., Hirabayashi, H., Morimoto, M., and Akabane, K. 1986, *Pub. Astr. Soc. Japan*, **38**, 475.
Steer, D. G., Dewdney, P. E., and Ito, M. R. 1984, *Astr. Ap.*, **137**, 159.
Thompson, A. R., Clark, B. G., Wade, C. M., and Napier, P. J. 1980, *Ap. J. Suppl.*, **44**, 151.
Ulvestad, J. S., and Wilson, A. S. 1984, *Ap. J.*, **285**, 439.
Unger, S. W., Pedlar, A., Booler, R. V., and Harrison, B. A. 1986, *M.N.R.A.S.*, **219**, 387.
van Gorkom, J. H., Schwarz, U. J., and Bregman, J. D. 1985, in *The Milky Way Galaxy*, ed. H. van Woerden, R. J. Allen, and W. B. Burton (Dordrecht: Reidel), p. 371.
Wakker, B. P., and Schwarz, U. J. 1988, *Astr. Ap.*, in press.
Whiteoak, J. B., Gardner, F. F., and Pankonin, V. 1983, *M.N.R.A.S.*, **202**, 11P.
Yusef-Zadeh, F., and Morris, M. 1987, *Ap. J.*, **320**, 545.
Yusef-Zadeh, F., Morris, M., and Chance, D. 1984, *Nature*, **310**, 557.
Yusef-Zadeh, F., Morris, M., Slee, O. B., and Nelson, G. J. 1986, *Ap. J. (Letters)*, **300**, L47.

K. R. ANANTHARAMAIAH: Raman Research Institute, Bangalore-560 080, India

W. M. GOSS and J. H. VAN GORKOM: NRAO-VLA, P.O. Box O, Socorro, NM 87801

R. D. EKERS: Australia Telescope, CSIRO, Epping, NSW 2121, Australia

A. PEDLAR: Nuffield Radio Astronomy Laboratories, Jodrell Bank, Macclesfield, Cheshire, SK11 9DL, UK

U. J. SCHWARZ: Kapteyn Astronomical Institute, Postbus 800, 9700 AV Groningen, The Netherlands

JUN-HUI ZHAO: University of New Mexico: Department of Physics and Astronomy, Albuquerque, NM 87131